Structural Characterization of the PawL-Derived Peptide Family, an Ancient Subfamily of Orbitides

Colton D. Payne[1], Mark F. Fisher[2,3], Joshua S. Mylne[2,3] and K. Johan Rosengren[1,]*

[1] The University of Queensland, School of Biomedical Sciences, Brisbane, QLD 4072, Australia

[2] The University of Western Australia, School of Molecular Sciences and The ARC Centre of Excellence in Plant Energy Biology, Crawley, WA 6009, Australia

[3] Curtin University, Centre for Crop and Disease Management, School of Molecular and Life Sciences, Curtin University, Bentley, WA 6102, Australia

KEYWORDS: orbitide, PawL-Derived Peptide (PLP), cyclic peptide, NMR structure

ABSTRACT:

Plants are an excellent source of bioactive peptides, often with disulfide bonds and/or a cyclic backbone. While focus has predominantly been directed at disulfide-rich peptides, a large family of small, cyclic but non-disulfide bonded peptides known as the orbitides has been relatively ignored. What research has been conducted has focused on discovering bioactive orbitides, with less attention to structural features. A recently discovered subfamily of the orbitides known as the PawL-Derived Peptides (PLPs) are produced during the maturation of precursors for seed storage albumins. Although their evolutionary origins have been dated, in-depth exploration of the family's structural characteristics and potential bioactivities remains to be conducted. Here we present an extensive characterization of the PLP family. Nine PLPs were produced by solid phase peptide synthesis. Although orbitides can have antimicrobial and therapeutic effects, none of these nine PLPs showed antibacterial or antifungal activity. Their structural features were studied using solution NMR spectroscopy and seven were found to possess regions of backbone order. Ordered regions consist of β-turns, with some PLPs adopting two well-defined β-turns within sequences as short as seven residues, which are largely the result of side chain interactions. Our data highlight that the sequence diversity within this family results in equally diverse shapes.

INTRODUCTION

Backbone head-to-tail cyclic peptides fall into many different families and can be found across all domains of life.[1-3] These peptides have been of particular interest for their structural stability and protease resistance conferred by the cyclization of their peptide backbones.[4, 5] In addition, many cyclic peptides also contain one or more disulfide bonds that provide an additional layer of support to both the structure and stability.[6]

Historically, cyclic peptides were discovered and isolated from plants based on bioactivity,[7, 8] but as their biosynthetic origins became known, transcriptomics has been favored for discovery as well as examining the genetic origins and processing mechanisms behind some of the cyclic peptide families.[9-11] Interestingly, several different head-to-tail cyclic peptide families share a processing and cyclization mechanism. These include the kalata-type cyclotides,[12] cyclic knottins[13] as well as the more recently discovered PawS-Derived Peptides (PDPs)[9] and PLPs,[14] all of which are proteolytically processed from precursor proteins by enzymes known as asparaginyl endopeptidases.[9, 12, 14]

Numerous members of the cyclotides, cyclic knottins and PDP families have had their 3D structures solved, and the features of these families are well established. Cyclotides and cyclic knottins adopt the cyclic cystine knot motif, an arrangement of disulfide bonds in which a ring like shape is formed by two disulfides, which brace the backbone of the peptide, with the knot 'tied' by the third disulfide bond threading through this ring.[15] Numerous bioactivities are reported for members of these families like uterotonic,[16] insecticidal,[17] and antimicrobial[18] activity as well as protease inhibition.[19] While most cyclotides are produced from dedicated precursor proteins,[20] some examples are encoded within precursor proteins for seed storage albumins.[12] This hijacking of an existing precursor protein already destined to be processed by

asparaginyl endopeptidases, is shared by the PDP family.[11] Most PDPs are cyclic peptides that adopt a single β-sheet separated by loops and bridged by a disulfide bond.[21] The prototypic member of the family, SFTI-1, has nanomolar potency as a trypsin inhibitor,[22] but little is known about the bioactivities and physiological roles of other members.

The 53 PLPs known to date are closely related to the PDPs, but lack disulfide bonds. Head-to-tail cyclic plant peptides without disulfide bonds are collectively referred to as orbitides, thus PLPs represent an evolutionary related subfamily of orbitides.[14] The orbitides have a range of biosynthetic origins, but are typically five to ten residue peptides with sequences mostly comprised of hydrophobic amino acids. X-ray crystallography has demonstrated that orbitides can adopt ordered turns, with the peptide backbone forming a stabilizing hydrogen bond network, however the total number of resolved structures remains low.[23] Orbitides reported over the course of the past two decades were often found due to a bioactivity such as antimalarial,[24] antifungal[25] or cytotoxic.[26] This research has yet to be extended in great detail to the PLPs. With both the knotted cyclic peptides and PDPs subjected to extensive research regarding function and structure, PLPs remain the last of the four structural families of head-to-tail cyclic peptides sharing this unique processing mechanism to be extensively structurally and functionally studied. Here we describe seven new solution NMR structures of PLPs and put their structural features into the context of observations of other orbitides, and we examine them for potential antimicrobial bioactivity.

RESULTS AND DISCUSSION

Chemical synthesis and purification of PLPs

A large number of PLP sequences have recently been discovered within albumin precursors of the Asteraceae family, 53 of which have been confirmed *in planta* via LC-MS/MS.[14, 27-29] This served to establish the existence of the PawL-derived Peptide subfamily of orbitides. To further the structural and functional understanding of the PLP family, nine PLPs of varying sequence lengths and compositions were chosen for study; these included PLPs -6, -13, -16, -22, -29, -31, -38, -42 and -46. The gene encoding each of these PLPs is known and the peptides are seven to ten amino acid residues in length, including an array of hydrophobic residues at varying locations (Figure 1). All contain a proto C-terminal Asp, and most have a proto N-terminal Gly residue typical of peptides cyclized by AEPs.[13] However, PLPs -6, -13 and -42 differ with the N-terminal residue being Phe for PLP-6 and Thr for PLPs -13 and -42.

Peptides were assembled in full on resin using fluorenylmethyloxycarbonyl (Fmoc)-based solid phase peptide synthesis. After synthesis all PLPs were cleaved from the resin whilst maintaining side chain protection, and cyclized in solution before side chain deprotection. Peptides were purified to >95 % by RP-HPLC and their identity confirmed by ESI-MS.

```
PLP-2        -------DLFVP-PID 8
PLP-4        ---------GLLGITD 7
PLP-6        --------FFDAAKID 8
PLP-10       ----------GSPLFD 6
PLP-12       --------FVGGTSFD 8
PLP-13       --------TFGVVIAD 8
PLP-16       --------GLFPYGPD 8
PLP-22       ---------GLPPYVD 7
PLP-29       --------GYFPVGVD 8
PLP-31       ------GVPFPLITHD 10
PLP-38       ---------GLYPYPD 7
PLP-42       -------TFFNP-VID 8
PLP-46       ---------GYITPLD 7
PLP-53       GSRIWVPGLGPVYEED 16
jatrophidin  ------PGLLNLWG-- 8
pohlianin C  ---TIIFGFGG----- 8
ribifolin    ---SIILGILG----- 8
xanthoxy D   -----GTVAVQFL--- 8
```

Figure 1: Alignment of PLPs and other orbitides. PLPs from this work (PLPs -6, -13, -16, -22, -29, -31, -38, -42 and -46) aligned with sequences for which structures are solved (PLPs -2,[14] -4,[14] -10,[14] -12[14] and -53[29] and orbitides jatrophidin,[23] pohlianin C,[23] ribifolin[23] and xanthoxycyclin D[30]). Negatively charged residues (Asp and Glu) and positively charged residues (Arg, His and Lys) are highlighted in red and blue respectively. Hydrophobic residues are highlighted in green.

NMR spectroscopy of PLPs

To date, five PLPs have been studied by solution NMR spectroscopy; these are PLPs -2, -4, -10, -12 and -53.[10, 29] PLP-2 was shown to have partially ordered structure, PLPs -4, -10 and -12 demonstrated a dynamic structure, and PLP-10 adopted at least two conformations based on proline isomerization. PLP-53, a uniquely large member of the PLP family at 16 residues in length, demonstrated a highly ordered region that had not been previously observed in the family. PLP-53 contains an extended turn region six residues in length, with the remaining ten residues forming a highly dynamic loop region.[29] These findings were in contrast to the PDP family whose members, similar in size, are highly structured due to their disulfide bonds.[21, 31, 32]

To further our understanding of the structural features adopted by the PLP family and potential key intramolecular interactions, PLPs -6, -13, -16, -22, -29, -31, -38, -42 and -46 were subjected to both homonuclear and heteronuclear solution NMR spectroscopy. As the majority of PLPs are comprised of almost entirely hydrophobic residues, with very few hydrophilic residues, many PLPs were insoluble in water. PLPs -6, -13, -22 and -31 were soluble in 90:10 H_2O/D_2O at varying concentrations. However, PLPs -16, -29, -38, -42 and -46 were insoluble at any concentration in 90:10 H_2O/D_2O and thus NMR samples of these peptides were prepared in either 50:50 H_2O/CD_3CN (PLPs -38 and -42), or 99.95% CD_3CN (PLPs -16, -29 and -46). The 1D spectra produced by the nine PLPs varied in dispersion and sharpness, with most demonstrating surprising dispersion for small peptides (Supporting Information). Usually, these features can be used to infer whether or not a peptide is adopting an ordered structure, with particularly wide dispersion of HN protons and sharp lines being strong indicators of a stable fold. Some PLPs have a markedly different 1D spectra to other members of the family; PLP-6 in particular demonstrated HN signals with low dispersion and notably broad peaks, indicating disorder and either partial aggregation or intermediate conformational exchange. In addition to this the 1D spectra of PLP-31 contained more signals than would be expected from its amino acid content, indicating the presence of multiple conformations in solution. Turning to the 2D data, for some of the PLPs few NOEs were observed leading to issues resolving and sequentially assigning spin systems. Due to the low molecular weight of the PLPs this is not surprising as there is typically minimal NOE buildup in peptides of this size due to their fast tumbling in solution. As ROE buildup is more likely to be effective in these molecules ROESY data were also recorded for the PLPs. However, little to no difference was observed in the data between the NOESY and ROESY spectra. Reducing the temperature from 298K to 283K also had no

significant effect on NOE buildup. However, sharp signals in the TOCSY and HSQC data allowed for the unambiguous assignment of almost all observed nuclei.

The chemical shifts of Hα and Cα/Cβ nuclei are sensitive to backbone torsion angles and commonly these nuclei are analyzed to identify the presence of secondary structure in a peptide.[33, 34] Thus, the Hα and Cα/Cβ chemical shifts for all PLPs were compared with random coil values (Figure 2 and Supporting Information). Chemical shifts that deviate substantially from the random coil values are indicative of ordered structure whereas values close to the random coil value are indicative of disorder. Typically, stretches of negative deviations are indicative of α-helical structure whereas stretches of positive deviation indicate β-sheet structure. Due to the short sequences of PLPs and the constrained cyclic backbone, it is unlikely that PLPs are able to adopt extensive secondary structure and thus these secondary shift graphs were used solely to indicate order or disorder. Hα secondary shifts that demonstrated strong deviations from random coil were found in PLPs -16, -29, -31, -38, -42 and -46 whereas the remaining PLPs had shifts that appeared closer to random coil. The HN, N, Hα, Cα and Cβ chemical shifts were used as input for the program Torsion Angle Likelihood Obtained from Shift and sequence similarity (TALOS-N)[35] to predict the backbone dihedral angles of the PLPs. TALOS-N predicted a number of dihedral angles for seven of the PLPs (-13, -16, -22, -29, -38, -42 and -46) indicating ordered regions in those peptides. In contrast, TALOS-N predicted that the backbones of PLP-6 and PLP-31 were dynamic. Although the Hα secondary shifts of PLP-31 appeared to suggest order, the Cα/Cβ showed very little deviation from random coil (Supporting Information), which is likely the basis for this prediction. As noted above PLP-31 adopts several conformations in solution and the data used for this analysis only reflects the dominant and fully assignable conformation. The large negative secondary Hα shift of Leu6 is more likely to be a

local ring current effect from the Phe4 sidechain rather than due to structural order of the backbone.

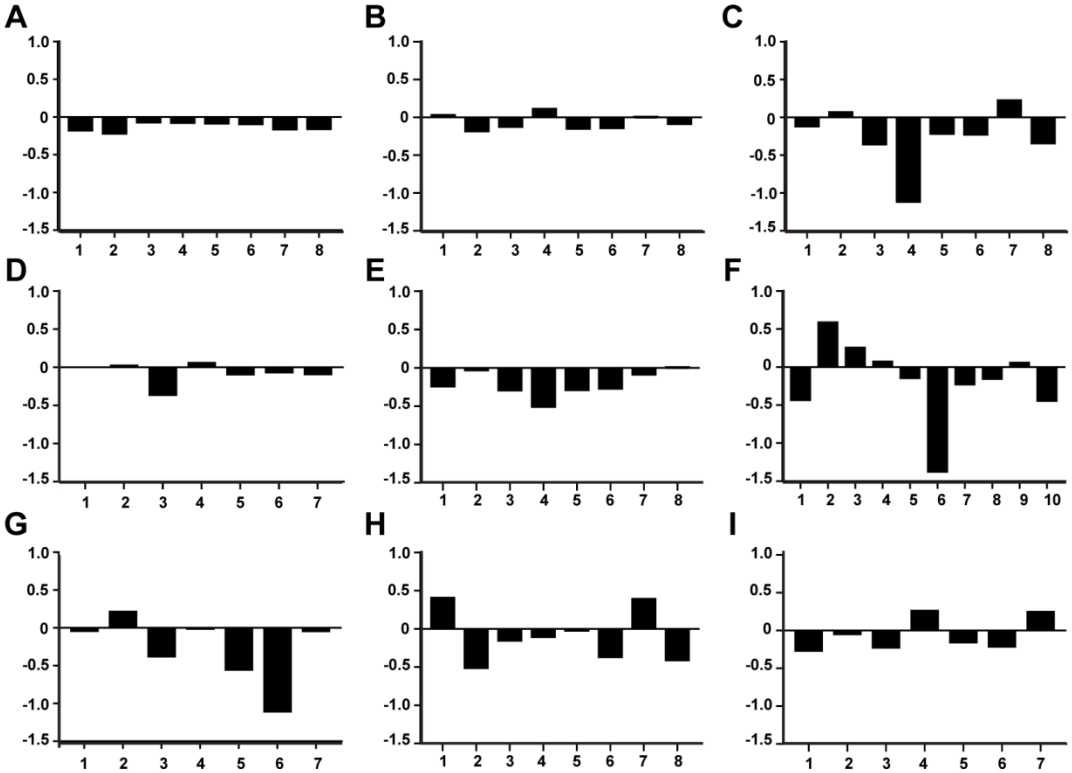

Figure 2: Secondary ^{1}Hα chemical shifts of PLPs. A-I: PLP-6, -13, -16, -22, -29, -31, -38, -42 and -46. Strong deviations from random coil (large positive or negative values) suggest order, whereas values close to zero suggest disorder. The y-axis for all graphs is the secondary chemical shift deviation (δΔ; ppm), the x-axis is the residue number.

Structure determination of PLPs

To evaluate the structural features of the PLPs, the 3D structures of PLP-13, -16, -22, -29, -38, -42, and -46 were determined using established protocols.[36] PLP-6 and PLP-31 were not analyzed further given the TALOS-N predictions of flexibility, and, in the case of PLP-31, the complexity of the data, which included several conformations. A combination of inter-proton distance restraints derived from NOESY cross peak volumes, backbone dihedral angle restraints

determined by TALOS-N, and hydrogen bond restraints based on temperature coefficients (Supporting Information) and preliminary structure calculations were used. Preliminary structures were calculated using automated NOE assignment with CYANA 3.98.5,[37] final structures were calculated and refined in explicit solvent using CNS 1.21.[38] All structures were analyzed using MolProbity[39] to assess their stereochemical quality by comparison to published structures. The best 20 structures from the calculated 50 based on MolProbity scores, low energy and no significant violations of the experimental data were chosen to represent the structural ensemble of each PLP (Figure 3, Table 1). All PLPs studied have good stereochemical quality with minimal to no Ramachandran outliers and atomic clashes. In addition, the backbone RSMD of all PLPs were below 0.3 Å in the ordered regions of the peptides.

Table 1: Structure Calculation Statistics of PLPs.							
Energies (kcal/mol)	**PLP-13**	**PLP-16**	**PLP-22**	**PLP-29**	**PLP-38**	**PLP-42**	**PLP-46**
Overall	-202.00 ± 7.75	-176.71 ± 4.92	-163.97 ± 3.76	-223.32 ± 15.36	-152.79 ± 16.38	-199.48 ± 14.73	-245.72 ± 3.98
Bonds	2.25 ± 0.35	1.80 ± 0.23	2.13 ± 0.38	2.29 ± 0.39	2.59 ± 0.36	2.26 ± 0.39	2.30 ± 0.26
Angles	8.25 ± 1.62	5.34 ± 0.98	9.78 ± 1.28	9.60 ± 2.70	11.05 ± 2.64	10.81 ± 2.18	7.91 ± 1.04
Improper	3.16 ± 1.99	2.50 ± 1.26	2.06 ± 0.76	2.86 ± 1.23	5.03 ± 2.20	4.34 ± 1.87	2.74 ± 0.43
Dihedral	32.69 ± 0.56	25.32 ± 0.40	24.33 ± 0.41	28.05 ± 0.54	25.04 ± 0.52	34.98 ± 0.60	26.85 ± 0.42
Van der Waals	-7.32 ± 3.15	-17.89 ± 2.47	-6.09 ± 2.08	-17.46 ± 3.64	-6.85 ± 2.76	-14.11 ± 2.72	-9.91 ± 2.26
Electrostatic	-241.11 ± 10.29	-193.85 ± 4.67	-196.19 ± 4.15	-248.66 ± 15.99	-190.05 ± 13.61	-238.06 ± 15.88	-275.99 ± 5.27
NOE	0.003 ± 0.004	0.002 ± 0.003	0.001 ± 0.002	0.003 ± 0.004	0.001 ± 0.008	0.001 ± 0.001	0.002 ± 0.002
cDih	0.067 ± 0.105	0.075 ± 0.089	0.003 ± 0.013	0.001 ± 0.005	0.381 ± 0.244	0.302 ± 0.285	0.395 ± 0.235
MolProbity Statistics							
Clashes (>0.4 Å/1000 atoms)	0.88 ± 2.70	1.32 ± 3.21	0.00 ± 0.00	3.56 ± 5.32	10.65 ± 8.10	1.16 ± 2.84	0.00 ± 0.00
Poor rotamers	0	0	0	0	0	0	0
Ramachandran outliers (%)	0	0	3.00 ± 7.33	0	0	0	0
Ramachandran favored (%)	90.00 ± 8.38	89.17 ± 11.18	76.00 ± 12.31	86.67 ± 11.60	95.00 ± 8.89	100.00 ± 0.00	85.00 ± 8.89
MolProbity score	1.01 ± 0.35	1.04 ± 0.38	1.21 ± 0.26	1.33 ± 0.56	1.56 ± 0.58	0.64 ± 0.34	1.06 ± 0.33
MolProbity score percentile	99.00 ± 1.12	98.75 ± 1.33	98.6 ± 0.99	91.75 ± 13.01	86.30 ± 16.77	99.55 ± 1.10	99.25 ± 0.44
Atomic RMSD (Å)							
Mean global backbone	0.66 ± 0.36	0.32 ± 0.11	0.40 ± 0.24	0.72 ± 0.39	0.66 ± 0.34	0.53 ± 0.24	0.16 ± 0.05
Mean global heavy	2.00 ± 0.73	1.75 ± 0.42	1.12 ± 0.30	1.86 ± 0.53	2.10 ± 0.71	1.96 ± 0.45	1.09 ± 0.47
Experimental Restraints							
NOE distances							
Short range (i – j < 2)	29	17	28	27	27	10	41
Medium range (i – j < 5)	10	1	7	2	1	2	3
Hydrogen bond restraints	6 (3 bonds)	0	2 (1 bond)	2 (1 bond)	0	4 (2 bonds)	10 (5 bonds)
Total	45	18	37	31	28	16	54
Dihedral Angle Restraints							
ϕ	3	2	1	1	3	5	3
ψ	3	4	2	2	3	6	4
Total	6	6	3	3	6	11	7
Violations							
NOE violations > 0.2 Å	0	0	0	0	0	0	0
Dihedral violations > 2.0°	0	0	0	0	0	0	0

Structural features of PLPs

PLPs, like other orbitides, are too small and constrained by their cyclic backbone to adopt secondary structures like α-helices and β-sheets. However, this does not mean that PLPs are unable to adopt any form of structural order. The small size of the PLPs enforces turns in which, hydrophobic interactions and intramolecular hydrogen bonds can stabilize the defined backbone conformations. These features were observed in all the PLPs for which 3D structures were calculated.

PLP-13, which was studied in water, is one of the more ordered members of the PLP family with two overlapping turns and three backbone hydrogen bonds. Two of the observed hydrogen bonds stabilize a type III β-turn comprising residue 4-7 and a type I β-turn comprising 5-8. These well-defined features established a global RMSD of 0.66 Å. The remaining hydrogen bond is between the HN proton of Thr1 and the backbone carbonyl of Ala7. These hydrogen bonds are all consistent with the amide temperature coefficients determined for PLP-13. The side chains of residues Ile6 and Ala7 participate in hydrophobic interactions with Val4, likely assisting in the stabilization of the two turns present in this region. Residues Phe2 and Gly3 are less defined and predicted by TALOS-N to be flexible. The side chains of Thr1, Phe2 and Asp8 are fully solvent-exposed.

Interestingly, no backbone hydrogen bonds were predicted for PLP-16. An atypical turn is formed by residues 4-7, based on backbone angles and the distance between Cα atoms, this is likely facilitated by the proline residues at positions 4 and 7. These two prolines, one of which is in a *cis* conformation (Pro4) and the other in a *trans* conformation (Pro7), also form a hydrophobic interaction with each other across the turn to further stabilize the backbone. Overall, this establishes a global RMSD of 0.32 Å. The remaining side chains, despite being large and

hydrophobic do not appear to participate in any interactions and are largely solvent-exposed, but it should be noted that the data for PLP-16 were recorded in 99.95% CD_3CN due to its poor solubility in water.

Two type III β-turns are formed in PLP-22 in water, one comprising residues 2-5 and the other residues 5-1, each supported by a backbone hydrogen bond. These turn regions are well-defined and establish a global RMSD of 0.40 Å. PLP-22 contains two sequential Pro residues at positions 3 and 4, both in the *trans* conformation and interestingly, all amino acid side chains, barring that of Val6, are projected on the same face of the PLP forming a densely packed hydrophobic surface.

PLP-29 only adopts only a single turn; a hydrogen bond between residues Pro4 and Val7 and hydrophobic contacts between the side chains of these residues stabilize a type II turn in this region. The remainder of the backbone of PLP-29 is less defined, but, the backbone folds back on top of itself, and achieves an RMSD of 0.72 Å. The remaining side chains, which are largely hydrophobic, project towards the solvent. Aromatic rings, when adjacent to a proline residue, can favor formation of a *cis* proline, but in this case the NMR data indicate Phe3 does not interact with Pro4 and that Pro4 is in the *trans* conformation.[40] Again, PLP-29 was studied in 99.95% CD_3CN because of its poor solubility in water. It cannot be ruled out that more defined packing of these side chains would occur in aqueous solution.

PLP-38 presents an interesting case wherein no hydrogen bonds were predicted and no turn region was observable. However, hydrophobic interactions between the side chains of residues Leu2 and Pro4 likely contribute to local order. Like PLP-16, the Pro4 and Pro6 residues in PLP-38 adopt different conformations; *trans* and *cis* respectively. Despite a lack of hydrogen bonding,

the global backbone RMSD of 0.66 Å suggests that PLP-38 has a stable conformation. The side chains are solvent exposed in 50:50 H_2O/CD_3CN.

PLP-42, like PLP-13, is a highly ordered member of the family with two hydrogen bonds stabilizing two consecutive turns: A type I turn is formed by residues 1-4 and a type III turn is formed by residues 4-7. This double turn creates highly ordered regions and establishes a global backbone RMSD of 0.53 Å, only allowing for some dihedral angle ambiguity at Thr1. No notable side chain interactions were present, with most side chains solvent-exposed based on the data recorded in 50:50 H_2O/CD_3CN.

PLP-46 is the most robustly stabilized member of the PLP family studied to date. PLP-46 contains five hydrogen bonds that fully constrain the backbone of the peptide, achieving a global backbone RMSD of 0.16 Å. Two of these hydrogen bonds between residues Gly1 and Thr4 and Thr4 and Asp7 form a double turn comprised of a type IV and a type III turn respectively, similar to what we observed in PLP-42. Intriguingly, the three remaining hydrogen bonds form between the backbone HN of residues Tyr2, Ile3 and Thr4 to the side chain OD1 and OD2 groups of Asp7. This places the side chain of Asp7 in a unique location, almost centralized perfectly over the cyclic ring of the backbone, allowing these protons to form hydrogen bonds with the side chain. All other side chains lack notable interactions and are solvent-exposed in 99.95% CD_3CN.

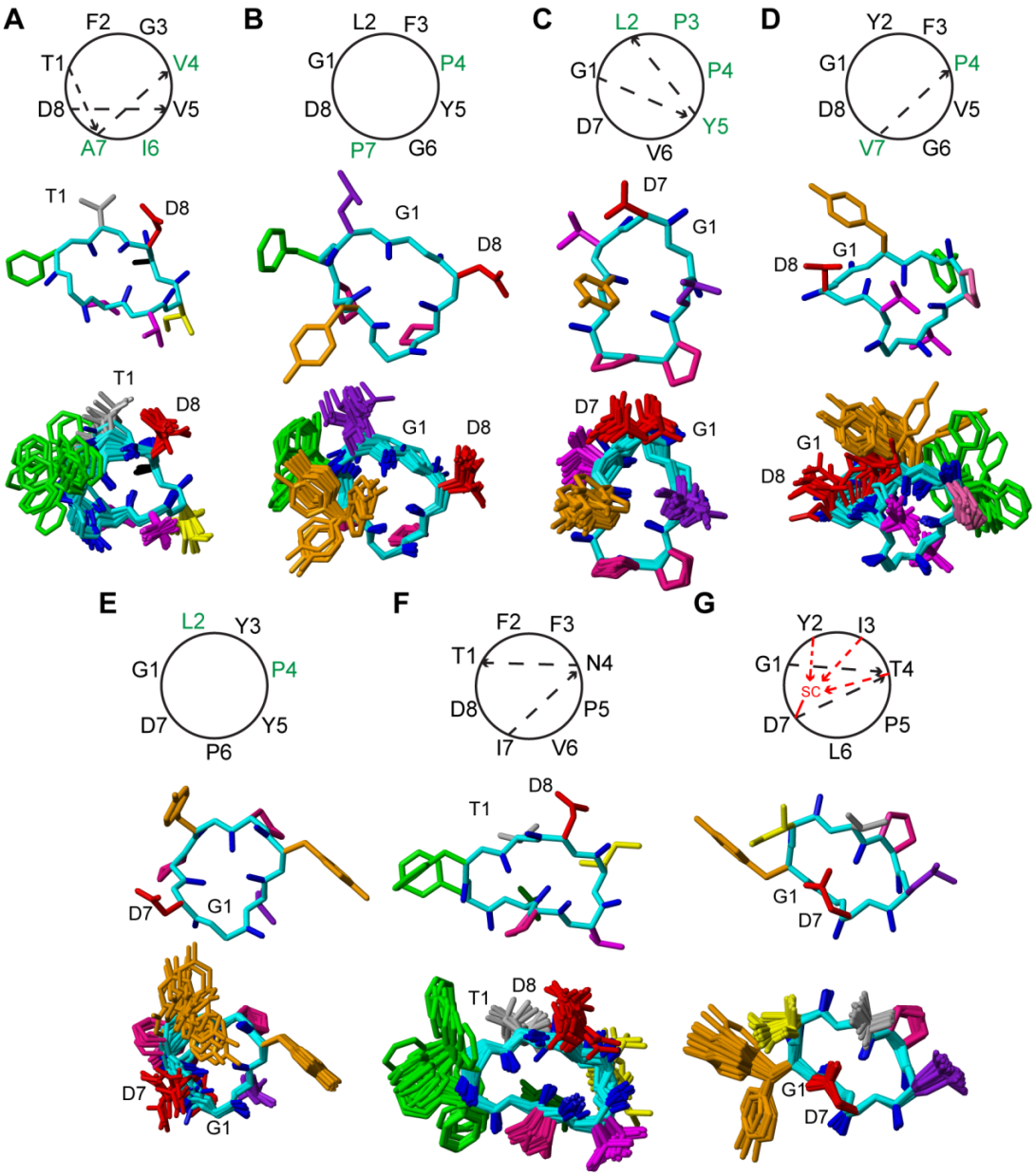

Figure 3: Hydrogen bond schematics and 3D structures of PLPs. A-G: PLP-13, -16, -22, -29, -38, -42 and -46. Hydrogen bonds are shown as dashed arrows (black arrows are from/to the peptide backbone, red arrows indicate hydrogen bonding to side chain groups). Green numbers indicate residues participating in hydrophobic side chain interactions. Three-dimensional structures are displayed with the backbone in cyan and the carbonyls in blue. Residues are colored as follows: Ala, black; Asn, dark green; Asp, red; Ile, yellow; Leu, purple; Phe, green; Pro, pink; Thr, grey; Tyr, orange; Val, magenta.

How structurally similar are PLPs to other orbitides?

CyBase[41] (a database of cyclic protein sequences) currently includes a total of 197 orbitide sequence entries, including the recently established 53 PLP sequences. Of these, eight orbitides have had their 3D structures solved by solution NMR spectroscopy or X-ray crystallography and the coordinates deposited in the Protein Data Bank (PDB). In addition to this, nine orbitides have had structures solved by X-ray crystallography and deposited in the Cambridge Structural Database.[23] Of the published orbitide structures, all contain at least one hydrogen bond stabilizing the backbone. Most of these hydrogen bonds stabilize turns, although some orbitides, like the PLPs studied here, contain other backbone-to-backbone or backbone-to-sidechain hydrogen bonds that further stabilize the peptide.

Intriguingly, most previously reported PLPs studied by NMR spectroscopy do not appear to adopt ordered structure in solution. Exceptions to this are PLP-2 and PLP-53. PLP-2 contains some order in a turn region, however, this is confined to three residues and likely due to two sequential proline residues locking its backbone configuration. The unusually large PLP-53 contains an extended turn region six residues in length with supporting hydrogen bonds.[29] Two peptides studied in this work, PLP-6 and PLP-31, were found to have dynamic structures based on chemical shifts, and thus are consistent with the structures of most previously reported PLPs. The remainder of the PLPs studied in this work, however, adopted more ordered structures consistent with what was observed throughout the rest of the orbitide family. PLPs, despite their small size, can adopt one or several highly ordered turns stabilized by hydrogen bonds and hydrophobic side chain interactions. These features are difficult to predict based on sequence alone and it is interesting to note that PLP-53, the largest reported PLP at 16 residues in length, only adopts a singular turn region, while PLPs half the size, such as PLPs -13, -22, -42 and -46,

adopt two turns. This work highlights that PLPs commonly adopt one or two ordered turn regions stabilized by hydrogen bonds and/or hydrophobic interactions, akin to other orbitides, further highlighting the PLPs position as a subfamily of the orbitides (Figure 4).

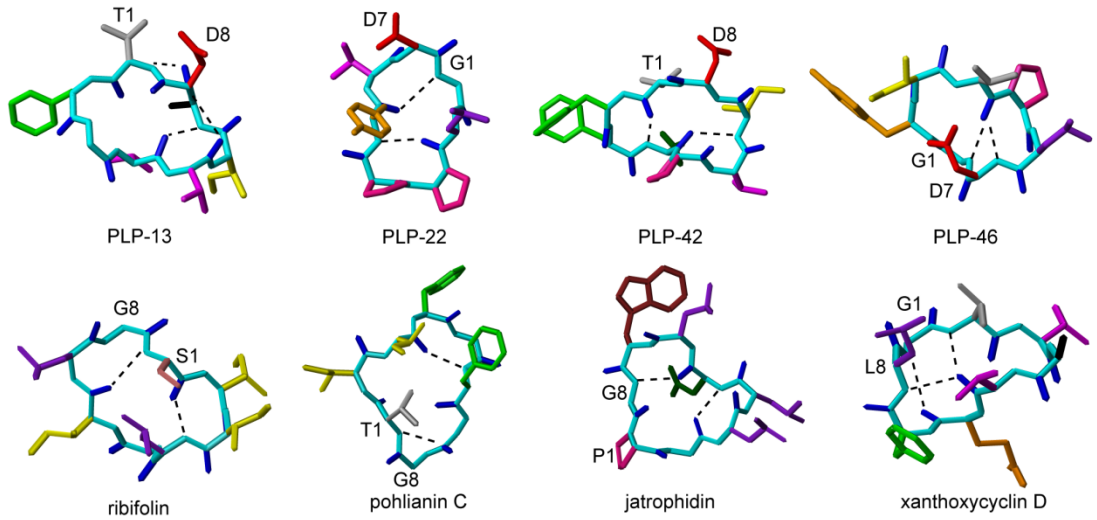

Figure 4: 3D structures of PLPs compared to other orbitides. Peptides are labeled beneath structures and are colored as described in Figure 3 with the additions of Gln in gold and Trp in brown. Backbone hydrogen bonding is shown with dashed lines. PLPs -13, -22, -42 and -46 are from this work. Ribifolin (6DKZ) from *Jatropha ribifolia*,[23] pohlianin C (6DL0) from *J. pohliana*,[23] jatrophidin (6DL1) from *J. curcas*[23] and xanthoxycyclin D (6WPV) from *Melicope xanthoxyloides*.[30]

Are PLPs antimicrobial?

Since some orbitides are reported to be antimicrobial, we tested our nine peptides for antifungal and antibacterial activity in a disc diffusion assay. Discs containing 200 µg of each PLP were placed on YPD (yeast extract, peptone and dextrose) agar plates swabbed with *C. albicans* and LB agar plates swabbed with either *Escherichia coli* K-12 or *Bacillus subtilis* Marburg No. 165. DMSO was the negative control and amphotericin B the positive control for

the fungal assays, DMSO and kanamycin for the bacterial assays. None of the PLPs tested inhibited the growth of bacteria (Supporting Information). The effect on *C. albicans* was also minimal, however PLP-29 did show minor inhibition of growth (Figure 5).

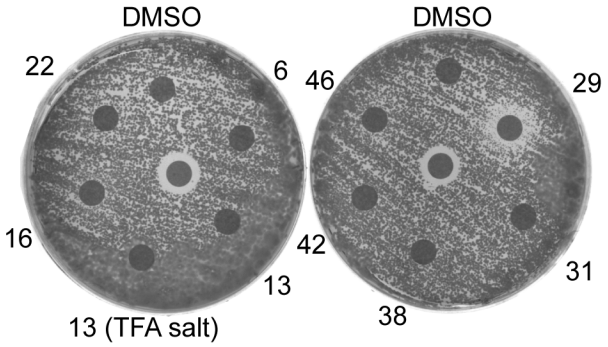

Figure 5: Disc diffusion assay of PLPs against *C. albicans*. Discs containing 200 μg of each PLP were placed on an YPD agar plates inoculated with *C. albicans*. A disc containing DMSO was used as a negative control and a disc containing 50 μg of amphotericin B (center) was used as a positive control. Most PLPs demonstrated no inhibition of fungal growth, although PLP-29 showed minor inhibition of *C. albicans*.

Given the potential activity of PLP-29 against *C. albicans* we performed a solution assay to determine its minimum inhibitory concentration. No measurable inhibition of growth was however observed at concentrations up to 640 μM (Supporting Information), whereas the amphotericin B positive control caused clear growth inhibition at 10 μM concentration. This result shows that PLP-29 is unlikely to have a useful antimicrobial function.

These results are consistent with a previous study which found that PLPs -2, -18 and -20 were not active against the Gram-positive bacteria *Bacillus cereus* and *Staphylococcus aureus*, nor against the Gram-negative bacteria *E. Coli* and *Pseudomonas aeruginosa*.[14]

Conclusion

In this work we have synthesized and characterized nine PLPs. None were found to inhibit the growth of fungi or bacteria, leaving their physiological roles yet to be understood. Structural characterization by NMR spectroscopy resulted in the determination of seven new structures displaying highly ordered turn regions. The remaining two (PLP-6 and PLP-31) have a dynamic backbone. This work highlights that the PLPs like other orbitides are restrained by backbone hydrogen bonds and side chain interactions. We show that the nature of these is diverse, highlighting the difficulty of predicting structure and dynamics of members of this family based on sequence alone.

EXPERIMENTAL SECTION

Peptide synthesis

PLPs were synthesized using Fmoc based solid phase peptide synthesis on 2-chlorotrityl resin at a 0.125 mmol scale. Loading of the C-terminal residue was achieved by dissolving 1 M eq. of the Fmoc-protected residue in minimal CH_2Cl_2 and 4 M eq. of N,N'-diisopropylethylamine (DIPEA) before addition of this solution to 2-chlorotrityl resin pre-swollen in dichloromethane for 1 h. Standard deprotection was conducted between couplings using 2 x 5 min reactions of 20% v/v piperidine in dimethylformamide (DMF). Subsequent amino acids were added to the peptide chain by activating 4 M eq. of the Fmoc protected amino acid in 4 M eq. of 0.5 M 2-(1H-benzotriazole-1-yl)-1,1,3,3-tetramethyluronium hexafluorophosphate and 8 M eq. of DIPEA and applying the solution to the resin using a CS336X peptide synthesizer (CSBio, CA, USA). Couplings were conducted twice for all amino acids that contain branched β-carbons or aromatic

rings. Upon completion of synthesis, peptides were cleaved from the resin using 10 x 3 min treatments of 2% (v/v) trifluoroacetic acid (TFA) in CH_2Cl_2 to maintain side chain protection. MeCN was added to the cleavage solution and rotary evaporation was conducted to remove the CH_2Cl_2 and TFA, with the remaining solution being lyophilized. Cyclization of the side chain protected PLPs was conducted in DMF at a 1 mM peptide concentration, 1 M eq. of 1-[bis(dimethylamino)methylene]-1H-1,2,3-triazolo[4,5-b]pyridinium 3-oxide hexafluorophosphate was added to this solution followed by the slow addition of 10 M eq. of DIPEA. The reaction was monitored over 2 h using electrospray ionization mass spectrometry (ESI-MS); phase separation with CH_2Cl_2 was used to isolate the peptide from the DMF after the reaction was completed. The CH_2Cl_2 containing the peptide was diluted with MeCN, then rotary evaporation was used to remove the CH_2Cl_2 and the peptide solution lyophilized. PLPs had side chain protection removed through deprotection using a solution of 97:2:1 TFA/H_2O/triisopropylsilane. The solution was stirred for 2 h before precipitation of the peptide using cold diethyl ether, the precipitate was filtered and re-dissolved in 50:50 MeCN/H_2O before lyophilization. All PLPs were purified using reverse phase high performance liquid chromatography (RP-HPLC) on a Prominence (Shimadzu, Rydalmere, AUS), crude purification was conducted on a C18 preparative column (300 Å, 10 μm, 21.2 mm i.d. x 250 mm, Phenomenex), ESI-MS was used to confirm the mass of the PLPs. Further purification was conducted using a semi-preparative C18 column (300 Å, 5 μm, 10 mm i.d. x 250 mm, Vydac) and purity was assessed with a C18 analytical column (300Å, 5 μm, 2.1 mm i.d. x 150 mm, Vydac). All purification was conducted using an increasing 1%/min gradient of 90:10 MeCN/H_2O, with all PLPs confirmed to be >95% pure.

NMR spectroscopy

NMR samples were prepared by dissolving 1-2 mg of peptide in 500 μL of solvent at pH ~3.5. PLPs -6, -13, -22 and -31 were dissolved in (90:10) H_2O/D_2O, PLP-38 and PLP-42 were dissolved in (50:50) H_2O/CD_3CN and PLPs -16, -29 and -46 were dissolved in 99.5% CD_3CN. One-dimensional as well as 2D ^1H-^1H TOCSY[42] and NOESY[43] experiments, with mixing times of 80 and 400 ms respectively, were recorded at 298 K on a 900 MHz Bruker Avance III spectrometer equipped with a cryoprobe. TOCSY experiments were recorded with 8 scans and 512 increments, NOESY experiments were recorded with 24-40 scans and 512 increments depending on signal-to-noise in the 1D spectra. Both TOCSY and NOESY data were recorded with a sweep width of 10 ppm due to the lack of Trp residues in PLP sequences. The ^1H-^{13}C and ^1H-^{15}N HSQC spectra were also recorded at 298 K at natural abundance. The ^1H-^{13}C experiments were recorded with 72 scans and 256 increments with a 10 ppm sweep width in the F2 dimension and an 80 ppm sweep width in the F1 dimension. The ^1H-^{15}N experiments were recorded with 128 scans and 128 increments with a sweep width of 10 ppm in the F2 dimension and 32 ppm in the F1 dimension. TOCSY temperature data were also recorded for all PLPs at 288, 293, 298, 303 and 308 K to monitor the temperature dependence of the amide protons. Data processing was conducted using Topspin 4.0.3 (Bruker) with the spectra being referenced to the solvent signal (spectra recorded at 298 K were referenced to the residual solvent at 4.769 ppm for H_2O/D_2O data and 2.031 for CD_3CN data). Sequential assignment strategies[44] were used to analyze all TOCSY and NOESY data; heteronuclear data were analyzed with the assistance of assigned TOCSY/NOESY data within the program CARA.[45] Secondary Hα/Cα/Cβ shifts were calculated via shift comparison to random coil values to determine order, if any, within the PLPs.[33]

Structure calculation

Inter-proton distance restraints were generated from the peak volumes of cross peaks present in the NOESY spectra for each PLP. TALOS-N[35] was used to predict dihedral ϕ (C_{-1}-N-Cα-C) and ψ (N-Cα-C-N_{+1}) backbone angles. Potential hydrogen bond donors were identified from backbone amide temperature coefficients. Values > -4.6 ppb/K for the coefficient of the linear relationship were taken to indicate a hydrogen bond donation by the particular HN proton.[46] Hydrogen bond acceptors were determined through preliminary structure calculations. Initial structures (50) were calculated in CYANA 3.98.5[37] using torsion angle simulated annealing, which defined the starting coordinates and distance restraints to be used in the CNS.[38] TALOS-N dihedral restraints, distance restraints from CYANA and hydrogen bonds from temperature coefficients were input into CNS 1.21.[38] A further 50 structures were generated in CNS by simulated annealing using torsion angles.[38] The annealed structures were then subjected to water minimization using Cartesian dynamics to generate final PLP structures. Stereochemical analysis was conducted by MolProbity via the comparison of the generated structures to previously published structures from RCSB.[39] MOLMOL[47] was used to display and generate images of structural ensembles with the 20 best structures, defined as having good geometry, no violations of distances of dihedral angles above 0.2 Å or 2° and low energy.

Antimicrobial disc diffusion assays

The nine peptides were each dissolved in DMSO to a concentration of 20 mg/mL for disc diffusion assays carried out using an existing protocol,[14] modified such that only one dose of each peptide was used. For the antibacterial assays, cultures of *E. coli* K-12 and *B. subtilis*

Marburg No. 165 in liquid LB medium were diluted to an OD_{600} of 0.1 and spread onto LB agar plates with a sterile swab. For antifungal assays with *C. albicans*, the same procedure was used except that a YPD culture was diluted to an OD_{600} of 0.05 and spread onto YPD agar plates.

Once the cultures had been absorbed by the medium, we dispensed 10 μL (200 μg) of each peptide onto sterile 8 mm filter paper discs and placed them on the inoculated plates. We also used discs containing 5 μL DMSO as a negative control on each plate. Positive controls were discs containing 50 μg of kanamycin for the antibacterial assays or 50 μg of amphotericin B for the antifungal assays. We hypothesized that the presence of TFA in the peptide samples (due to chemical synthesis) might have an effect on the assay. To control for this we removed any traces of TFA from all the peptides, via salt exchange with HCl, prior to dissolving them in DMSO. One aliquot of PLP-13 was left untreated for the purposes of comparison. The cultures were incubated at 37 °C for 16 h (bacteria) or 20 h (fungus), then inspected for any inhibition of microbial growth.

Antifungal minimum inhibitory concentration assay

To confirm the antifungal activity of PLP-29, we performed an assay to determine its minimum inhibitory concentration. Onto a 96-well plate we dispensed 200 μL aliquots of *C. albicans* in YPD medium containing PLP-29 to a final concentration of 5, 10, 20, 40, 80, 160, 320 or 640 μM in three replicates. Further cultures containing amphotericin B as a positive control were dispensed in the same concentrations, again in three replicates. A series of negative control cultures contained DMSO to the same concentrations as the PLP-29 and amphotericin B samples (both amphotericin B and PLP-29 were initially dissolved in DMSO before further dilution with water). A “no inoculum” series of controls contained growth medium and PLP-29 only, in the same concentrations as above. After measuring the initial OD_{595} of each well with a

FLUOstar OPTIMA plate reader (BMG Labtech GmbH, Offenburg, Germany), the plate was incubated for 7 h at 37 °C, after which the final OD_{595} was measured. Fungal growth was measured by the change of optical density over time, comparing the wells containing DMSO only with those containing either PLP-29 or amphotericin B.

Author Information

Corresponding Author

E-mail: j.rosengren@uq.edu.au (K.J.R.) Tel: +61 7 33651403

Author Contribution

C.D.P.: peptide chemistry, NMR data analysis, structure calculations. M.F.F.: antifungal and antibacterial assays. J.S.M. and K.J.R. project design and funding. C.D.P. K.J.R and M.F.F wrote the manuscript with input from J.S.M.

Acknowledgements

This work was supported by Australian Research Council (ARC) grants DP120103369 and DP19190102058 to J.S.M. and K.J.R. C.D.P. was supported by a UQ postgraduate research award. K.J.R. and J.S.M were supported in part by ARC Future Fellowships FT130100890 and FT1201000013 respectively. This work utilized the Queensland NMR Network 900 MHz NMR spectrometer.

Conflicts of interest

The authors declare no competing financial interests.

References

1. Göransson, U.; Burman, R.; Gunasekera, S.; Strömstedt, A. A.; Rosengren, K. J., Circular proteins from plants and fungi. *J. Biol. Chem.* **2012,** 287, (32), 27001-27006.

2. Lehrer, R. I.; Cole, A. M.; Selsted, M. E., θ-Defensins: cyclic peptides with endless potential. *J. Biol. Chem.* **2012,** 287, (32), 27014-27019.

3. Montalbán-López, M.; Sánchez-Hidalgo, M.; Cebrián, R.; Maqueda, M., Discovering the bacterial circular proteins: bacteriocins, cyanobactins, and pilins. *J. Biol. Chem.* **2012,** 287, (32), 27007-27013.

4. Wang, C. K.; Craik, D. J., Designing macrocyclic disulfide-rich peptides for biotechnological applications. *Nat. Chem. Biol.* **2018,** 14, (5), 417-427.

5. Bhardwaj, G.; Mulligan, V. K.; Bahl, C. D.; Gilmore, J. M.; Harvey, P. J.; Cheneval, O.; Buchko, G. W.; Pulavarti, S. V. S. R. K.; Kaas, Q.; Eletsky, A.; Huang, P. S.; Johnsen, W. A.; Greisen, P., Jr.; Rocklin, G. J.; Song, Y.; Linsky, T. W.; Watkins, A.; Rettie, S. A.; Xu, X.; Carter, L. P.; Bonneau, R.; Olson, J. M.; Coutsias, E.; Correnti, C. E.; Szyperski, T.; Craik, D. J.; Baker, D., Accurate *de novo* design of hyperstable constrained peptides. *Nature* **2016,** 538, (7625), 329-335.

6. Conibear, A. C.; Rosengren, K. J.; Daly, N. L.; Henriques, S. T.; Craik, D. J., The cyclic cystine ladder in θ-Defensins is important for structure and stability, but not antibacterial activity. *J. Biol. Chem.* **2013,** 288, (15), 10830-10840.

7. Gran, L., Oxytocic principles of *Oldenlandia affinis*. *Lloydia* **1973,** 36, (2), 174-8.

8. Gustafson, K. R.; Sowder, R. C.; Henderson, L. E.; Parsons, I. C.; Kashman, Y.; Cardellina, J. H.; McMahon, J. B.; Buckheit, R. W.; Pannell, L. K.; Boyd, M. R., Circulins A and B. Novel human immunodeficiency virus (HIV)-inhibitory macrocyclic peptides from the tropical tree *Chassalia parvifolia*. *JACS* **1994,** 116, (20), 9337-9338.

9. Elliott, A. G.; Delay, C.; Liu, H.; Phua, Z.; Rosengren, K. J.; Benfield, A. H.; Panero, J. L.; Colgrave, M. L.; Jayasena, A. S.; Dunse, K. M.; Anderson, M. A.; Schilling, E. E.; Ortiz-Barrientos, D.; Craik, D. J.; Mylne, J. S., Evolutionary origins of a bioactive peptide buried within preproalbumin. *Plant Cell* **2014,** 26, (3), 981-995.

10. Bernath-Levin, K.; Nelson, C.; Elliott, A. G.; Jayasena, A. S.; Millar, A. H.; Craik, D. J.; Mylne, J. S., Peptide macrocyclization by a bifunctional endoprotease. *Chem. Biol.* **2015,** 22, (5), 571-582.

11. Mylne, J. S.; Colgrave, M. L.; Daly, N. L.; Chanson, A. H.; Elliott, A. G.; McCallum, E. J.; Jones, A.; Craik, D. J., Albumins and their processing machinery are hijacked for cyclic peptides in sunflower. *Nat. Chem. Biol.* **2011,** 7, (5), 257-259.

12. Poth, A. G.; Colgrave, M. L.; Lyons, R. E.; Daly, N. L.; Craik, D. J., Discovery of an unusual biosynthetic origin for circular proteins in legumes. *PNAS* **2011,** 108, (25), 10127.

13. Mylne, J. S.; Chan, L. Y.; Chanson, A. H.; Daly, N. L.; Schaefer, H.; Bailey, T. L.; Nguyencong, P.; Cascales, L.; Craik, D. J., Cyclic peptides arising by evolutionary parallelism via asparaginyl-endopeptidase-mediated biosynthesis. *Plant Cell* **2012,** 24, (7), 2765-2778.

14. Fisher, M. F.; Zhang, J.; Taylor, N. L.; Howard, M. J.; Berkowitz, O.; Debowski, A. W.; Behsaz, B.; Whelan, J.; Pevzner, P. A.; Mylne, J. S., A family of small, cyclic peptides buried in preproalbumin since the Eocene epoch. *Plant Direct* **2018,** 2, (2), 1-17.

15. Craik, D. J.; Daly, N. L.; Bond, T.; Waine, C., Plant cyclotides: A unique family of cyclic and knotted proteins that defines the cyclic cystine knot structural motif. *J. Mol. Biol.* **1999,** 294, (5), 1327-1336.

16. Koehbach, J.; O'Brien, M.; Muttenthaler, M.; Miazzo, M.; Akcan, M.; Elliott, A. G.; Daly, N. L.; Harvey, P. J.; Arrowsmith, S.; Gunasekera, S.; Smith, T. J.; Wray, S.; Göransson, U.; Dawson, P. E.; Craik, D. J.; Freissmuth, M.; Gruber, C. W., Oxytocic plant cyclotides as templates for peptide G protein-coupled receptor ligand design. *PNAS* **2013,** 110, (52), 21183-21188.

17. Jennings, C.; West, J.; Waine, C.; Craik, D.; Anderson, M., Biosynthesis and insecticidal properties of plant cyclotides: the cyclic knotted proteins from *Oldenlandia affinis*. *PNAS* **2001,** 98, (19), 10614-9.

18. Malik, S. Z.; Linkevicius, M.; Göransson, U.; Andersson, D. I., Resistance to the cyclotide cycloviolacin O2 in *Salmonella enterica* caused by different mutations that often confer cross-resistance or collateral sensitivity to other antimicrobial peptides. *Antimicrob. Agents Chemother.* **2017,** 61, (8).

19. Chiche, L.; Heitz, A.; Gelly, J. C.; Gracy, J.; Chau, P. T.; Ha, P. T.; Hernandez, J. F.; Le-Nguyen, D., Squash inhibitors: from structural motifs to macrocyclic knottins. *Curr. Protein Pept. Sci.* **2004,** 5, (5), 341-349.

20. Dutton, J. L.; Renda, R. F.; Waine, C.; Clark, R. J.; Daly, N. L.; Jennings, C. V.; Anderson, M. A.; Craik, D. J., Conserved structural and sequence elements implicated in the processing of gene-encoded circular proteins. *J. Biol. Chem.* **2004,** 279, (45), 46858-67.

21. Elliott, A.; Franke, B.; Armstrong, D.; Craik, D.; Mylne, J.; Rosengren, K. J., Natural structural diversity within a conserved cyclic peptide scaffold. *Amino Acids* **2017,** 49, 103-116.

22. Franke, B.; Mylne, J. S.; Rosengren, K. J., Buried treasure: biosynthesis, structures and applications of cyclic peptides hidden in seed storage albumins. *Nat. Prod. Rep.* **2018,** 35, (2), 137-146.

23. Ramalho, S. D.; Wang, C. K.; King, G. J.; Byriel, K. A.; Huang, Y.-H.; Bolzani, V. S.; Craik, D. J., Synthesis, racemic X-ray crystallographic, and permeability studies of bioactive orbitides from *Jatropha* species. *J. Nat. Prod.* **2018,** 81, (11), 2436-2445.

24. Pinto, M. E. F.; Batista, J. M.; Koehbach, J.; Gaur, P.; Sharma, A.; Nakabashi, M.; Cilli, E. M.; Giesel, G. M.; Verli, H.; Gruber, C. W.; Blanch, E. W.; Tavares, J. F.; da Silva, M. S.; Garcia, C. R. S.; Bolzani, V. S., Ribifolin, an orbitide from *Jatropha ribifolia*, and its potential antimalarial activity. *J. Nat. Prod.* **2015,** 78, (3), 374-380.

25. Tian, J.; Shen, Y.; Yang, X.; Liang, S.; Shan, L.; Li, H.; Liu, R.; Zhang, W., Antifungal cyclic peptides from *Psammosilene tunicoides*. *J. Nat. Prod.* **2010,** 73, (12), 1987-1992.

26. Cândido-Bacani, P. d. M.; Figueiredo, P. d. O.; Matos, M. d. F. C.; Garcez, F. R.; Garcez, W. S., Cytotoxic orbitide from the latex of *Croton urucurana*. *J. Nat. Prod.* **2015,** 78, (11), 2754-2760.

27. Behsaz, B.; Mohimani, H.; Gurevich, A.; Prjibelski, A.; Fisher, M.; Vargas, F.; Smarr, L.; Dorrestein, P. C.; Mylne, J. S.; Pevzner, P. A., *De novo* peptide sequencing reveals many cyclopeptides in the human gut and other environments. *Cell Syst*. **2020,** 10, (1), 99-108.e5.

28. Jayasena, A. S.; Fisher, M. F.; Panero, J. L.; Secco, D.; Bernath-Levin, K.; Berkowitz, O.; Taylor, N. L.; Schilling, E. E.; Whelan, J.; Mylne, J. S., Stepwise evolution of a buried inhibitor peptide over 45 My. *Mol. Biol. Evol*. **2017,** 34, (6), 1505-1516.

29. Fisher, M. F.; Payne, C. D.; Rosengren, K. J.; Mylne, J. S., An orbitide from *Ratibida columnifera* seed containing 16 amino acid residues. *J. Nat. Prod*. **2019,** 82, (8).

30. Fisher, M. F.; Payne, C. D.; Chetty, T.; Crayn, D.; Berkowitz, O.; Whelan, J.; Rosengren, K. J.; Mylne, J. S., The genetic origin of evolidine, the first cyclopeptide discovered in plants, and related orbitides. *J. Biol. Chem*. **2020,** 295, (42), 14510-14521.

31. Franke, B.; Jayasena, A. S.; Fisher, M. F.; Swedberg, J. E.; Taylor, N. L.; Mylne, J. S.; Rosengren, K. J., Diverse cyclic seed peptides in the Mexican zinnia (*Zinnia haageana*). *Biopolymers* **2016,** 106, (6), 806-817.

32. Payne, C. D.; Franke, B.; Fisher, M. F.; Hajiaghaalipour, F.; McAleese, C. E.; Song, A.; Eliasson, C.; Zhang, J.; Jayasena, A. S.; Vadlamani, G.; Clark, R. J.; Minchin, R. F.; Mylne, J. S.; Rosengren, K. J., A chameleonic macrocyclic peptide with drug delivery applications. *Chem. Sci*. **2021,** 12, 6670-6683.

33. Wishart, D.; Bigam, C.; Holm, A.; Hodges, R.; Sykes, B., 1 H, 13 C and 15 N random coil NMR chemical shifts of the common amino acids. I. Investigations of nearest-neighbor effects. *J. Biomol. NMR* **1995,** 5, (1), 67-81.

34. Wishart, D. S.; Case, D. A., Use of chemical shifts in macromolecular structure determination. In *Methods in enzymology*, Academic Press: 2002; Vol. 338, pp 3-34.

35. Shen, Y.; Bax, A., Protein backbone and sidechain torsion angles predicted from NMR chemical shifts using artificial neural networks. *J. Biomol. NMR* **2013,** 56, (3), 227-241.

36. Schroeder, C. I.; Rosengren, K. J., Three-dimensional structure determination of peptides using solution nuclear magnetic resonance spectroscopy. In *Snake and Spider Toxins: Methods and Protocols*, Priel, A., Ed. Springer US: New York, NY, 2020; pp 129-162.

37. Güntert, P., Automated NMR structure calculation with CYANA. *Methods Mol. Biol.* **2004,** 278, 353-378.

38. Brünger, A. T.; Adams, P. D.; Clore, G. M.; Delano, W. L.; Gros, P.; Grosse-Kunstleve, R. W.; Jiang, J. S.; Kuszewski, J.; Nilges, M.; Pannu, N. S.; Read, R. J.; Rice, L. M.; Simonson, T.; Warren, G. L., Crystallography & NMR system: A new software suite for macromolecular structure determination. *Acta Crystallogr D Biol. Crystallogr.* **1998,** 54, 905-921.

39. Chen, V. B.; Arendall, r. W. B.; Headd, J. J.; Keedy, D. A.; Immormino, R. M.; Kapral, G. J.; Murray, L. W.; Richardson, J. S.; Richardson, D. C., MolProbity: all-atom structure validation for macromolecular crystallography. *Acta Crystallogr. D* **2010,** 66, (Pt 1), 12-21.

40. Rosengren, K. J.; Daly, N. L.; Plan, M. R.; Waine, C.; Craik, D. J., Twists, knots, and rings in proteins. Structural definition of the cyclotide framework. *J. Biol. Chem.* **2003,** 278, 8606-8616.

41. Wang, C. K. L.; Kaas, Q.; Chiche, L.; Craik, D. J., CyBase: a database of cyclic protein sequences and structures, with applications in protein discovery and engineering. *Nucleic Acids Res*. **2007,** 36, 206-210.

42. Braunschweiler, L.; Ernst, R. R., Coherence transfer by isotropic mixing: Application to proton correlation spectroscopy. *J. Magn. Reson*. **1983,** 53, (3), 521-528.

43. Jeener, J.; Meier, B. H.; Bachmann, P.; Ernst, R. R., Investigation of exchange processes by two dimensional NMR spectroscopy. *J. Chem. Phys*. **1979,** 71, (11), 4546-4553.

44. Wüthrich, K., *NMR of proteins and nucleic acids*. New York : John Wiley & Sons: 1986.

45. Keller, R. L. J., *The computer aided resonance assignment tutorial*. 1 ed.; CANTINA Verlag: 2004.

46. Cierpicki, T.; Otlewski, J., Amide proton temperature coefficients as hydrogen bond indicators in proteins. *J. Biomol. NMR* **2001,** 21, (3), 249-261.

47. Koradi, R.; Billeter, M.; Wüthrich, K., MOLMOL: A program for display and analysis of macromolecular structures. *J. Mol. Graphics* **1996,** 14, 51-55.